IEEE Access, Volume 6, pp. 77529 - 77541
DOI: 10.1109/ACCESS.2018.2883379

Date of publication xxxx 00, 0000, date of current version xxxx 00, 0000.

Digital Object Identifier 10.1109/ACCESS.2017.Doi Number

Highly Efficient Wearable CPW Antenna Enabled By EBG-FSS Structure for Medical Body Area Network Applications

Adel Y.I. Ashyap[1], Z. Z. Abidin[1], Member, IEEE, S. H. Dahlan[1], Member, IEEE, H. A. Majid[1], Member, IEEE, M. R. Kamarudin[2], Senior Member, IEEE, A. Alomainy[3], Senior Member, IEEE, Raed A. Abd-Alhameed[4], Jamal Kosha[4], Senior Member, IEEE, James M Noras[4]

[1]Center for Applied Electromagnetic (EMCenter), Faculty of Electrical and Electronic Engineering, Universiti Tun Hussein Onn Malaysia, (UTHM) Batu Pahat 86400, Johor, Malaysia.
[2]Centre for Electronic Warfare, Information and Cyber, Cranfield Defence and Security, Cranfield University, Defence Academy of the United Kingdom, Shrivenham, SN6 8LA, UK.
[3] Antennas and Electromagnetics Research Group, School of Electronic Engineering and Computer Science, Queen Mary University of London, London E1 4NS, U.K.
[4] Faculty of Engineering and Informatics, University of Bradford, Bradford, BD7 1DP, UK

Corresponding authors: Muhammad Ramlee Kamarudin (e-mail: Ramlee.Kamarudin@cranfield.ac.uk) and Zuhairiah Zainal Abidin (e-mail: zuhairia@uthm.edu.my).

ABSTRACT A wearable fabric CPW antenna is presented for Medical Body Area Network (MBAN) applications at 2.4 GHz, based on an electromagnetic band-gap design and frequency selective surface (EBG-FSS). Without EBG-FSS the basic antenna has an omnidirectional radiation pattern, and when operated close to human tissue, the performance and efficiency degrade, and there is a high Specific Absorption Rate (SAR). To overcome this problem, the antenna incorporates EBG-FSS which reduces the backward radiation, with SAR reduced by 95%. The gain is improved to 6.55 dBi and the front to back ratio (FBR) is enhanced by 13 dB compared to the basic antenna. The overall dimensions of the integrated design are 60 × 60 × 2.4 mm^3. Simulation and experimental studies reveal that the antenna integrated with EBG-FSS can tolerate loading by human tissue as well as bending. Thus, the design is a good candidate for MBAN applications.

INDEX TERMS AMC, EBG, SAR, wearable fabric antennas.

I. INTRODUCTION

Medical Body Area Networks (MBAN) are becoming a vital technology in wearable systems, with applications in telemetry and medicinal services. MBAN is utilized to observe the health of patients at home, in hospital or even at outpatient surgeries. The important parameters of health are measured using implanted and wearable systems, which permit a continuous and unobtrusive examination of patients' state of health, for example monitoring blood pressure, ECG, EEG, or heart rate. The performance of the MBAN relies on the efficiency of the wireless communication devices, which need to be light-weight, low-profile, miniaturized, efficient, flexibly conforming to the shape of the human body, and capable of giving continuous monitoring. They must also ensure dependable communication within their networks.

The antenna is key to the wireless communication system and dictates its operation. Designing narrowband and robust wearable antennas, with acceptable efficiency and performance is a challenging task, particularly when the antennas are expected to possess lightweight, low-profile and conformal characteristics [1-11].

Positioning the antenna near a lossy medium such as the human body causes performance reduction, since capacitive coupling between the human body and the antenna alters the operating frequencies and the input impedance of the antenna. Also, the radiation efficiency of the antenna is expected to diminish due to the absorption of some power by the body tissue, and changes in the radiation pattern can result in transmission errors [8-10]. In order to be useful in MBAN, antennas must be able to function well close to

human tissue, with very low radiation toward the body to meet the specific absorption rate (SAR) limit.

To date, quite a few wearable antennas have been introduced operating at the demand frequency of 2.4 GHz, with and without the integration of flexible materials. Aside from coplanar waveguide (CPW) antennas [12-14], traditional patches, slot patches and monopole antennas [15-18], subsequent versatile antenna designs with improved efficiency and performance have appeared. Magneto-electric dipole antennas [19] and substrate-integrated waveguide antennas [20-23] have been designed based on fabric materials, showing either dual-band or single-band operation. At the same time, monopoles [24] and inverted-F fabric antennas [25, 26] have been well documented. They are small in area, yet may increase SAR levels when working near to body tissue, because of their nearly bi-directional radiation patterns. In an endeavor to diminish the effect of human tissue loads and enhance the isolation, High Impedance Surface (HIS) designs have been presented and implemented using either semi-flexible or flexible materials [27-36]. The HIS designs attain high degrees of isolation between the antennas and the body tissues. However, these proposed designs have the drawbacks of large footprints and may be too thick and big for MBAN applications [27-33], use semi-flexible material that is not adequately bendable and may not be comfortable for users [34, 35]. They may also show a frequency shift due to bending or poor front to back ratio (FBR) [29, 32, 36].

Generally, electromagnetic wave radiation is deemed unsafe for human tissue health. Furthermore, when an antenna is near to the body, it is influenced by the human body's biological organization. Therefore, there are strict standards for SAR defined for Europe or the US to follow.

Accordingly, to reduce SAR below the safety limits, an electromagnetic band-gap (EBG) has been used [27-36], since EBG could eliminate most of the electromagnetic energy in the desired frequency bands. In this study, a fabric CPW antenna integrated with EBG-FSS structures is designed and studied to determine its benefits and safety. The antenna incorporating EBG-FSS is thinner than in previous work as compared in Table I [27-36]; in addition, its SAR values are reduced significantly and the antenna gain enhanced.

This paper is arranged as follow: Section II discusses the CPW antenna and EBG designs, with CST software [37] employed in examining the antenna's size and electric properties; Section III covers the integration of the CPW antenna with EBG and investigates performance in free space as well as the impacts of placing EBG and PEC over the antenna; Section IV considers the behavior of the design when it is bent and loaded on the human body, with distances between the design and tissues varied to study the impacts on performance and SAR; finally Section V concludes with the achievements of the design.

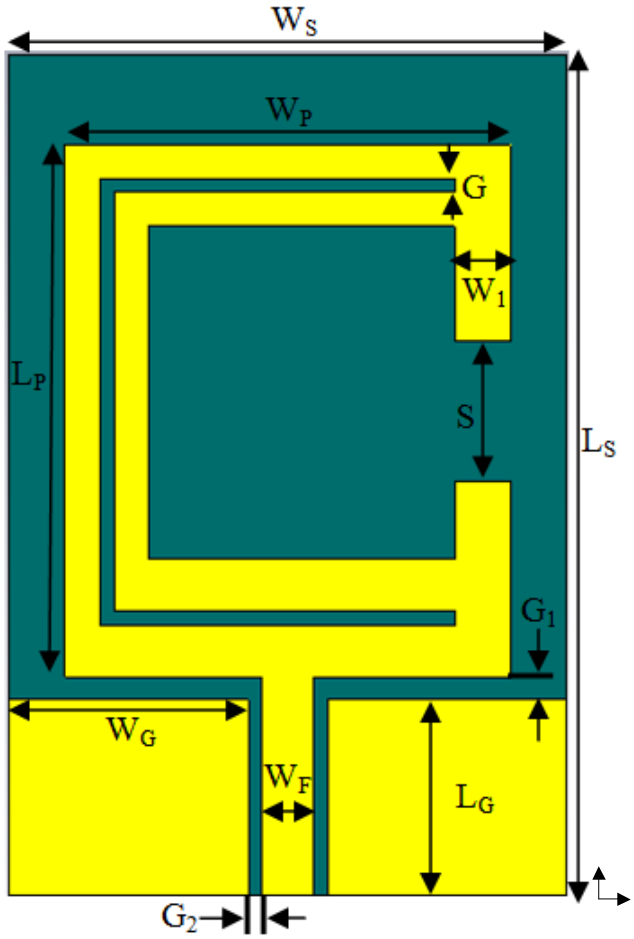

FIGURE 1. Front view of the fabric CPW antenna. The optimized dimensions are L_S = 30 mm, Ws = 20 mm, Wp = 16 mm, Lp = 19 mm, W_1 = 2 mm, G = 0.5 mm, G_1 = 0.8mm, G_2 = 0.5 mm, S = 5 mm, LG = 7 mm, W_G = 8.57 mm, and W_F = 1.86 mm.

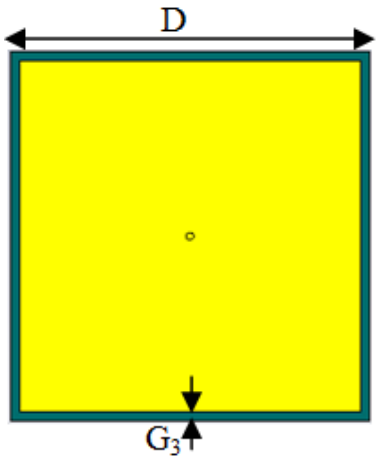

FIGURE 2. Conventional Sievenpiper EBG. The optimized dimension is D = 48 mm, G_3 = 1.2 mm and via = 0.5 mm.

TABLE I
COMPARISON OF PREVIOUS WEARABLE ANTENNA WITH PRESENTED DESIGN

Ref	Number of unit cell	Gain (dBi)	Dimensions (mm3)	Bandwidth (%)	SAR(w/kg) 1 g	10 g	Distance from the body	Reflected plane	Substrate type
[27]	6× 4	7	318×212×7	9.52	N/A	N/A	N/A	AMC	Felt/flexible
[28]	3×3	6.4	120 ×120 ×4.3	4	0.079	0.043	5.3	EBG	Felt/flexible
[29]	3×3	7.3	81×81×4	14.7	0.554	0.2	6	EBG	Felt /Flexible
[30]	3×3	N/A	150 ×150×4	5.08	N/A	0.016	1	EBG	Jeans / Flexible
[31]	2×2	5.2	50×50×5	11.3	0.13-0.18	N/A	4	HIS	PDMS/ Flexible
[32]	3 × 3	4.8	65.7×65.7× 3.3	18	0.683	N/A	N/A	AMC	Kapton polyimide for antenna and viny for AMC/ Flexible
[33]	3 × 3	N/A	72×72×5	9.2	1.57	0.37	N/A	Metamaterial	Polyimide/ Flexible
[34]	1×2	6.88	68×38× 6.57	5	0.244	N/A	2	EBG	RT/duroid 5880 /Semi-flexible
[35]	2×2	6.2	62 × 42 × 4	5.5	0.79	N/A	1	Metsurface	Rogers RO3003 /Semi-flexible
[36]	4 × 4	2.5	100×100×4.5	N/A	N/A	0.0464	10	AMC	Felt/Flexible
This paper	2×2	6.55	60×60×2.4	8.3	0.055	N/A	1	EBG-FSS	jeans/flexible

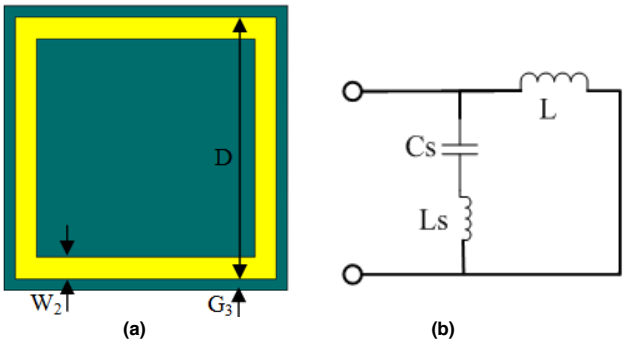

FIGURE 3. (a) Square loop based on EBG-FSS and (b) equivalent circuit of (a). The optimized dimensions are D = 27.6 mm, G_3 = 1.2 mm, and W_2 = 2.25 mm.

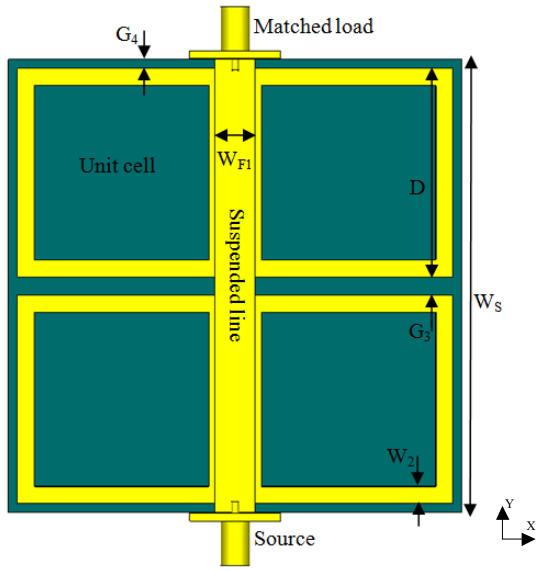

FIGURE 4. Technique of suspended microstrip line to evaluate band-gap. The optimized dimensions are Ws =60 mm, D = 27.6 mm, G_3 = 2.4 mm, G_4 = 1.2 mm, W_2 = 2.25 mm, and W_{F1} = 5.32 mm.

II. DESIGNS OF ANTENNA AND EBG STRUCTURES

A. Dimension and Size Design

A wearable textile antenna is designed as shown in Fig.1. It is C-shaped, additionally etched with a C-slot. This slot on the radiator element is to obtain compactness in size. A coplanar waveguide is fed at the bottom of the substrate, with a signal strip of width W_F and two gaps of G_2. Two rectangular patches beneath the radiating elements support the antenna as ground planes. The CPW feeding method reduces the fabrication complexity of the antenna, because both the ground planes and the radiator are positioned on the top of the dielectric.

Jeans material (denim) with a thickness of 0.7 mm, a loss tangent of 0.07 and a relative permittivity of 1.7 provided the supporting dielectric substrate. To achieve 50 Ω characteristic impedance, the size of the width W_F, the gap G_2, and other dimensions are critical. The overall size of the antenna is 30×20×0.7 mm^3. The working frequency band was selected as 2.4 GHz for MBAN applications.

B. Square loop EBG STRUCTURE

The traditional Sievenpiper EBG is illustrated in Fig. 2. The desired frequency is calculated based on equation (1) [38]. It is realized that the unit cell has the overall dimensions of 48×48×0.7 mm^3. In order to form an array of 2×2, the overall dimension will increase to 96 ×96×0.7 mm^3. This dimension is considered electrically large; therefore, it is desired to reduce the conventional dimensions.

$$f = \frac{1}{2\pi\sqrt{LC}} \quad (1)$$

An increment in the capacitance or the inductance of the structures lowers the frequency. However, increasing the capacitance diminishes the bandwidth. Hence, it is better to increase the inductance instead of the capacitance of the

structure. The inductance can be increased without increasing the capacitance by using a thick substrate, but a thicker substrate takes more space and enlarges the systems. A different approach is to employ a frequency selective surface (FSS) through a series LC equivalent circuit model rather than a traditional patch. In this case, the desired frequency is given by equation (2) [32],[39], which shows that the total structural inductance increases due to the additional surface inductance. Hence, it is necessary to use the high-inductance FSS as a top layer rather than a traditional patch that behaves as a capacitive surface. A design that has this type of model with significant inductance is called a square loop, and is shown in Fig. 3 (a) [39]. Note that there are several FSS structures with series LC models that have a significant inductance. However, the majority of structures are complex or have vias, and vias and complexity are not preferable in designing for fabric materials and might lead to inaccuracy.

$$f = \frac{1}{2\pi\sqrt{(L+L_S)C_S}} \tag{2}$$

A demonstration of 2×2 array square loop FSS-EBG has been studied and verified through simulation and measurement of an equivalent circuit. The finite integrated method is used to design this EBG-FSS structure in CST. In order to have a low-profile design, the EBG-FSS is constructed on 0.7 mm thickness of denim, the same as the CPW antenna substrate. The equivalent circuit model of the designed textile square-loop is inspired from [32],[35],[39]-[41] as illustrated in Fig. 3(b). It is an LC series circuit where the capacitance (Cs) is due to the gap size between horizontal conductor and calculated by the following equation (3)[3],[42].

$$C_S = \frac{W\varepsilon_0(1+\varepsilon_r)}{\pi} cosh^{-1}\left(\frac{W+g}{g}\right) \tag{3}$$

where W is the perimeter dimensions of the unit-cell conductive material, and g is the gap size between the two adjacent unit-cells.

The inductance (Ls) comes from the loop metal conductors and calculated by the following equation (4)[43].

$$L_S = \ell_n \frac{\mu_0}{4\pi} ln\left\{1 + \frac{32h^2}{w_n^2}\left[1 + \sqrt{1 + \left(\frac{\pi w_n^2}{8h^2}\right)^2}\right]\right\} \tag{4}$$

where ℓ is the length of the strip, h is the substrate thickness and w is the width of the strip.

The inductance L is the load and given by the following equation [42].

$$L = \mu_0 h \tag{5}$$

where μ is permeability, h is the substrate

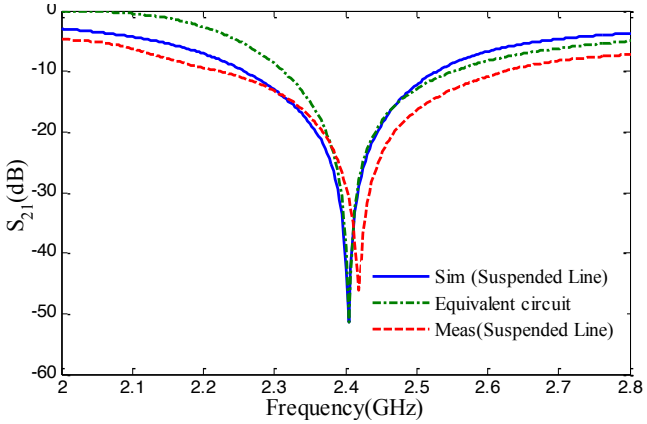

FIGURE 5. S_{21} band-gap characteristics based on suspended line technique and equivalent circuit.

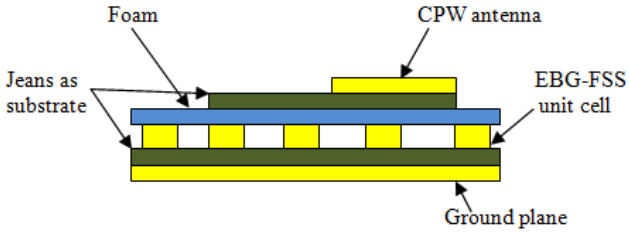

(a)

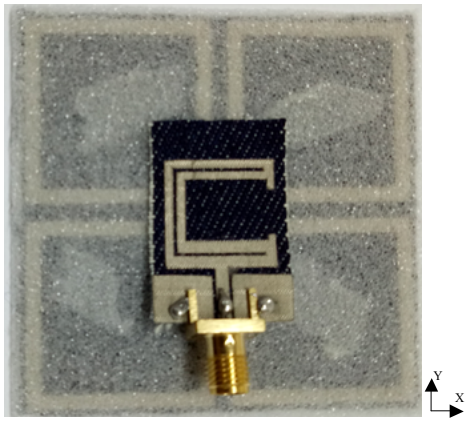

(b)

FIGURE 6. Antenna over EBG-FSS: (a) side view of the integrated design and (b) fabricated design.

The technique of a suspended microstrip line [44] is utilized to study the band-gap features of the square loop EBG-FSS structures, as depicted in Fig. 4. The EBG-FSS array is placed between the suspended line and ground, forming a sandwich-like structure. The suspended line is placed between two waveguides during simulation and soldered with two SMA connectors during measurements to evaluate the S_{21} parameters. Compared with traditional monopoles and coplanar microstrip techniques, the suspended line is a robust coupling structure, lessening the impact of other parasitic propagation modes. The band-gap features of the EBG-FSS are revealed more clearly.

Fig. 5 depicts the comparative results of the EBG-FSS unit cell based on the suspended line technique with the equivalent circuit, which is the result of the equivalent circuit is obtained from the ADS software. Only S_{21} is shown for clarity. A particular stop-band is seen with resonant frequency of 2.4 GHz. The range of frequency with S_{21} less than -10 dB [45] extends for the three cases from 2.25 GHz to 2.53 GHz.

III. INTEGRATION OF ANTENNA WITH EBG-FSS

A. Antenna performance with EBG-FSS

Once the textile CPW antenna and EBG-FSS have been designed separately, the textile CPW antenna is combined with EBG-FSS, using as a separation between them 1 mm thick foam, with permittivity of 1.05 and loss tangent of 0.0003. This separation is optimum, giving the antenna integrated with EBG-FSS the best S_{11}. Fig. 6 (a) illustrates the configuration of the integrated design.

Note that with the antenna placed over the EBG-FSS, a mutual impedance coupling arises between them [46]. This could cause detuning of the resonant frequency. Therefore, to obtain the desired resonant frequency as well as a better reflection coefficient, the dimension of the radiation patch is modified as seen in Fig. 6 (b). Here the length of the patch Lp is reduced by 3 mm, W_1 by 1 mm and S is increased by 1.5 mm. Fig. 7 illustrates the simulation and measurement results of S_{11} of the antenna alone and when placed on EBG-FSS. The figure shows sensible agreement between simulated and measured results below -10 dB. There is a slight shift in the measured S_{11} to higher frequency in the case of antenna with EBG-FSS and a slight shift to lower frequency with the antenna alone. This difference could be attributable to the accuracy of the fabrication process. Furthermore, integrating antenna with EBG shows better reflection coefficient compared to antenna alone. The result agrees with [29].

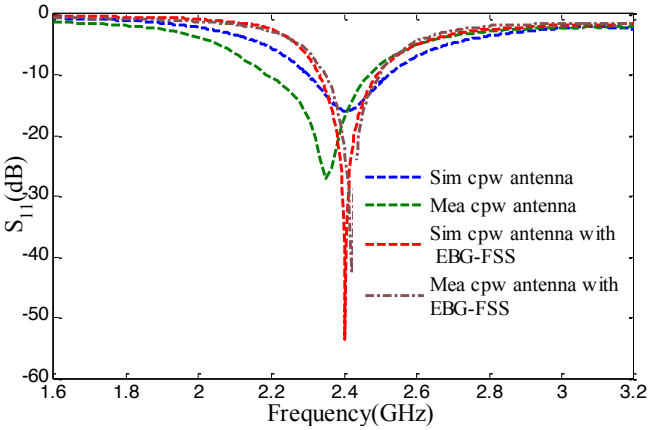

FIGURE 7. CPW antenna with and without EBG-FSS

The simulation and measurement of the radiation pattern of the antenna with and without the EBG-FSS backing in the H-plane and the E-plane are illustrated in Fig. 8. The experiment was conducted in an anechoic chamber. It is seen that the antenna without EBG-FSS has an omnidirectional pattern in its H-plane and a dipole-like pattern in its E-plane. In other words, the antenna gives maxima along the negative and positive z-axis indicating significant backward radiation. However, integrating the EBG-FSS with the basic antenna leads to a good FBR increase and a higher maximum gain compared with the antenna alone, and decreases the back radiation toward the body by around 13 dB whereas the antenna gain increases from 1.74 dBi to 6.55 dBi, all at 2.4 GHz. Most importantly, the usefulness of the EBG-FSS is achieved without vias and for a small size of 2×2 elements.

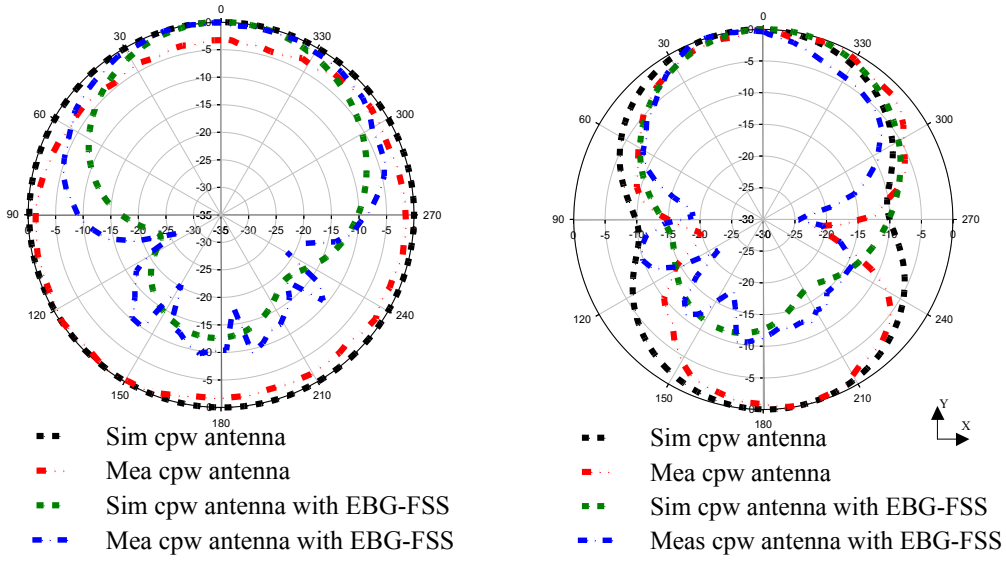

FIGURE 8. The radiation pattern of CPW antenna alone and integrated with EBG-FSS in (a) the H-plane (b) the E-plane.

B. Antenna performance over EBG-FSS and PEC

Experimental studies between the ordinary metal (PEC) and periodic EBG-FSS structure are carried out to show the usefulness of EBG-FSS. Fig. 6 (b) and Fig. 9 illustrates the placement of the antenna over EBG-FSS and PEC respectively. To compare fairly, the textile antenna is placed over EBG-FSS and PEC with the same height and dimensions, and in the case of PEC, the experimental studies use the same substrate as EBG-FSS. Fig. 10 displays the experimental results: when the antenna is above PEC as ground plane the reflection coefficient of the antenna has a value greater than -10 dB which almost linear. This is because the ordinary metal surface has 180^0 phase with a λ/4 spacing between the metal and the antenna, which results in opposing directions of the current of the antenna and the image current of the PEC, causing in a very poor return loss. Furthermore, adding EBG-FSS to the antenna shows a good reflection coefficient at 2.4 GHz. This is due to the phase behavior of the EBG-FSS ensuring that the image current and the original current flow in the same direction giving a constructive result. Overall, the antenna with PEC demonstrates a poorer impedance matching, as indicated by S_{11} greater than -10 while the antenna integrated with EBG-FSS shows much better impedance matching with S_{11} less than -10 dB at 2.4 GHz. Therefore, EBG appears a good choice for a wearable low-profile antenna.

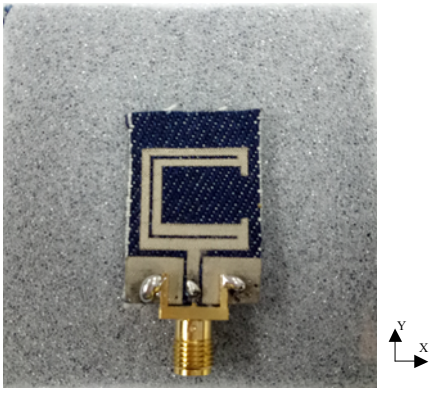

FIGURE 9. Antenna over PEC

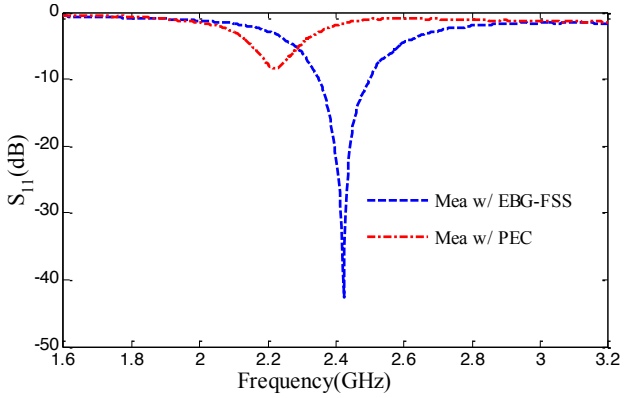

FIGURE 10. Experimental S_{11} of the CPW antenna on EBG-FSS and PEC as ground planes, respectively.

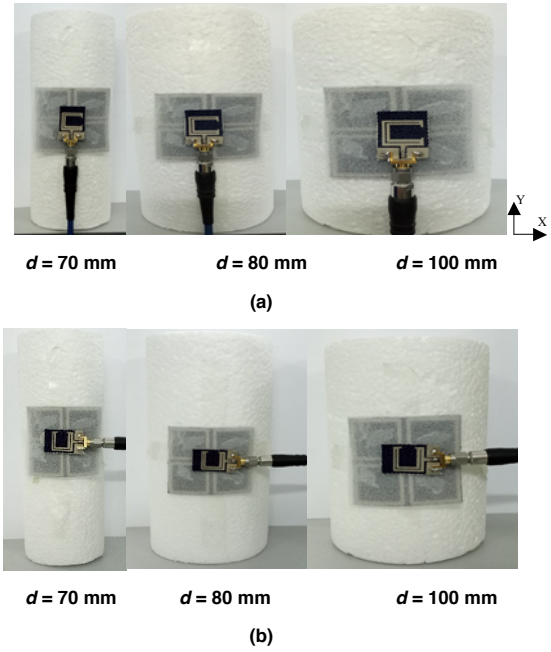

FIGURE 11. Bending process along (a) y-axis and (b) x-axis

IV. BEHAVIOR OF THE DESIGN ON BODY

A. Bending Evaluation

In several applications, the wearable antenna is anticipated to be deformed or conformed to human body surfaces during operation, to make sure that the operating frequency and general characteristics are maintained under bending, as when being worn. Therefore, before examining the human body loading impact, firstly an investigation on the integrated antenna with EBG-FSS under different degrees of structural deformations in free space is desired to ensure its consistency, with curvatures induced using polystyrene cylinders (ε_r) with three different diameters of curvature values, namely 70 80 and 100 mm, as illustrated in Fig. 11. They are chosen based on typical human leg, arm and chest sizes. Adhesive tape is used to fix the antenna on the polystyrene cylinder.

The experimental results of bending along the y-axis (as shown in Fig. 11(a)) with three diameter values are described in Fig. 12 (a). It is clear that the desired frequency band and bandwidth are maintained < -10 dB. There is a slight shift to higher frequency operation as the diameter is decreased. With increasing diameter, S_{11} appears more stable as seen in the case of d = 100 mm, but overall the frequency shifts are negligible as the desired frequency band is maintained < -10 dB.

Bending along the x-axis is carried out similarly as illustrated in Fig. 11 (b). The experimental result is illustrated in Fig. 12 (b), and here the effects are greater compared to the case of the y-axis. In case of d = 70 mm, the shift is about 30 MHz upwards while with d = 80 mm, the shift is about 25 MHz downwards. With d = 100 mm the resonant frequency is almost unaffected. Overall, the shifts in frequency still may

be considered negligible since the desired frequency still is < –10 dB. The greater effect with the x-axis bending may be due to the current distributions changing along the strip line, affecting the resonant length.

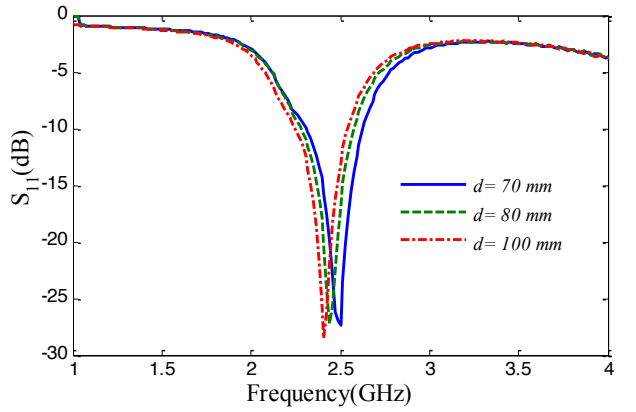

(a)

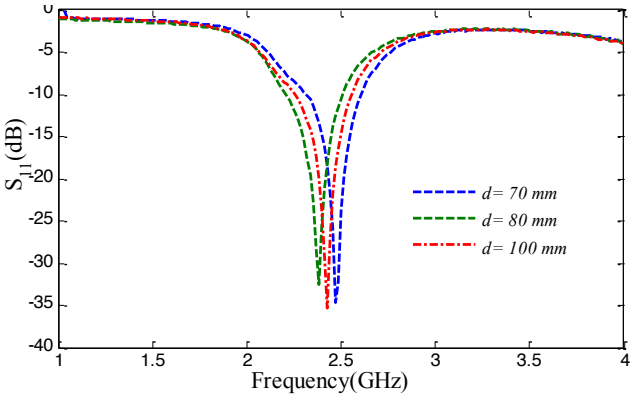

(b)

FIGURE 12. Measured S_{11} under bending along (a) y-axis and (b) x-axis.

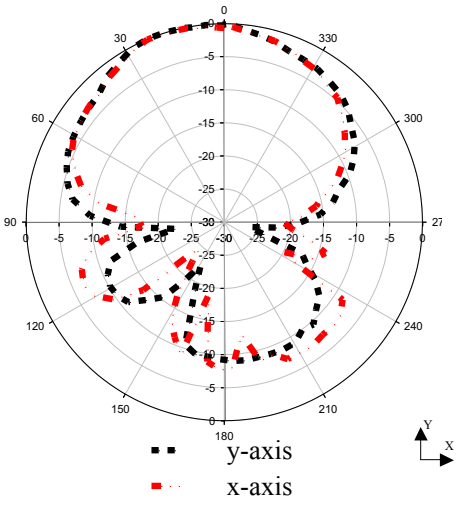

FIGURE 13. Measured radiation patterns under bending with d = 100 mm.

Next, the radiating performance of the antenna integrated with EBG-FSS under bending conditions is investigated. The experimental studies are carried out for one bending direction for each radiating plane. The bending is along the y-axis for the y-plane pattern and along the x-axis for the x-plane pattern with d = 100 mm. The integrated antenna was conformably positioned on the cylinder using tape. The experimental results, see Fig. 13, show that the antenna retains good radiating performance, and that the radiating characteristics are insensitive to bending. The bending has a slight effect, namely in increasing the back radiation. The slight asymmetry could be due to the position of the foam separator that may affect the cable movement during the measurement, because of a non-uniformity across the integrated structure during bending.

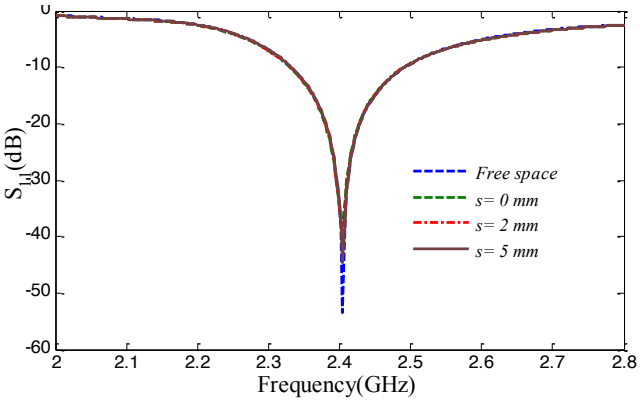

(a)

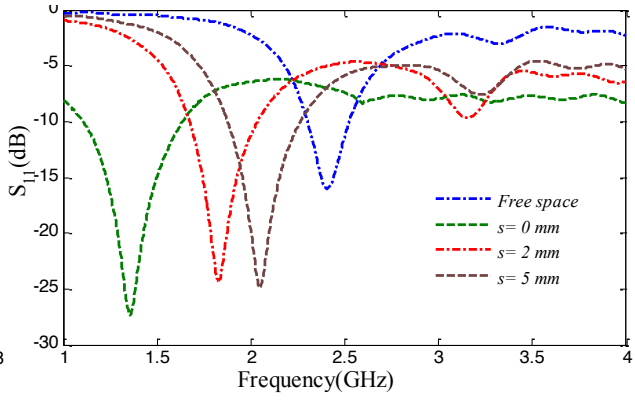

(b)

FIGURE 14. Simulated S_{11} behavior for (a) antenna integrated with EBG-FSS and (b) antenna alone on multilayer tissue model representing human chest.

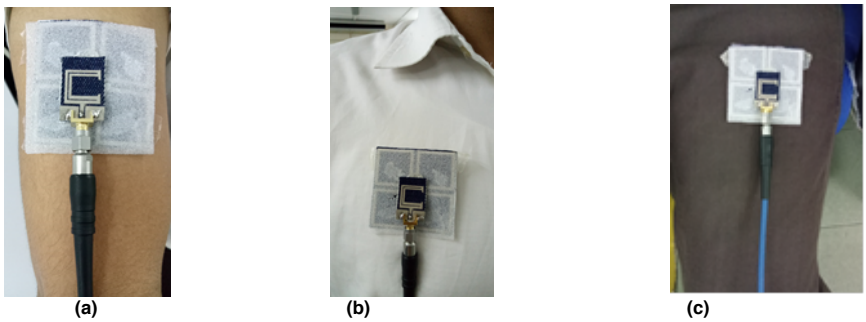

(a) (b) (c)

FIGURE 15. Antenna placement on different parts of human body: (a) arm, (b) chest and (c) leg.

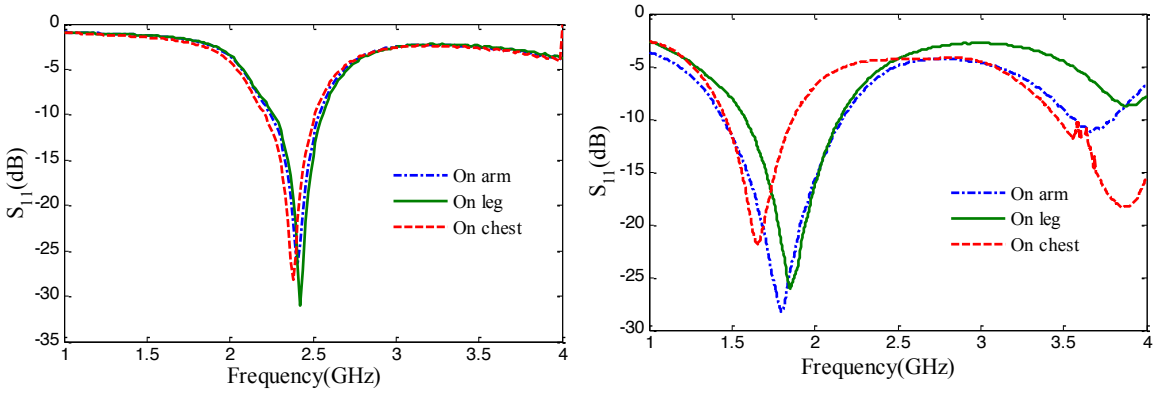

(a) (b)

FIGURE 16. Measured S_{11} behavior on human body for (a) antenna integrated with EBG-FSS and (b) antenna alone.

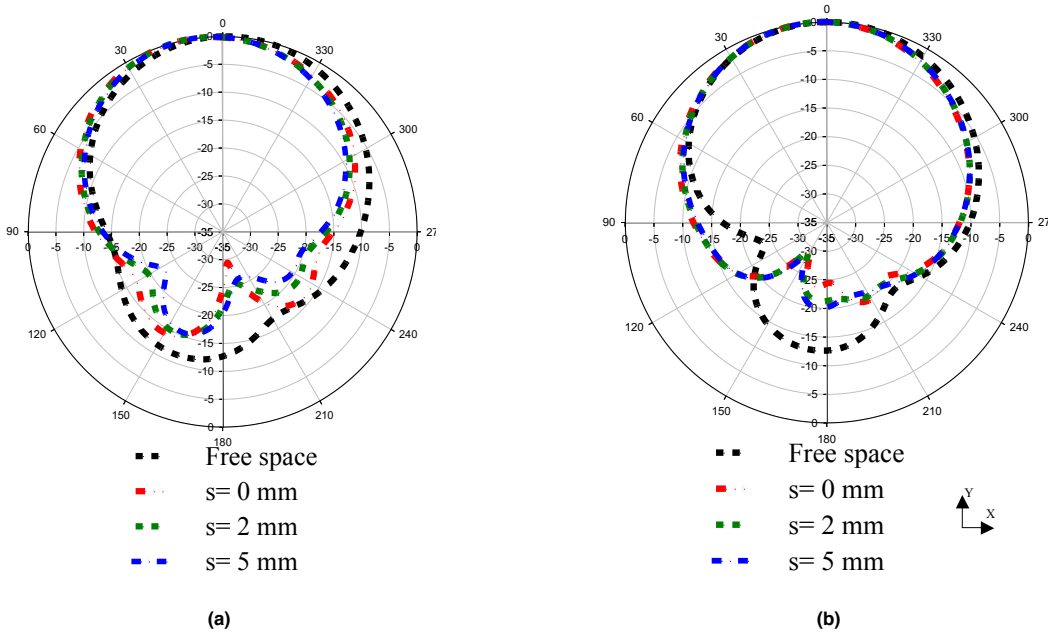

(a) (b)

FIGURE 17. Radiation patterns of the integrated antenna with varying distance from the multilayer tissue model in the (a) E-plane and (b) H-plane.

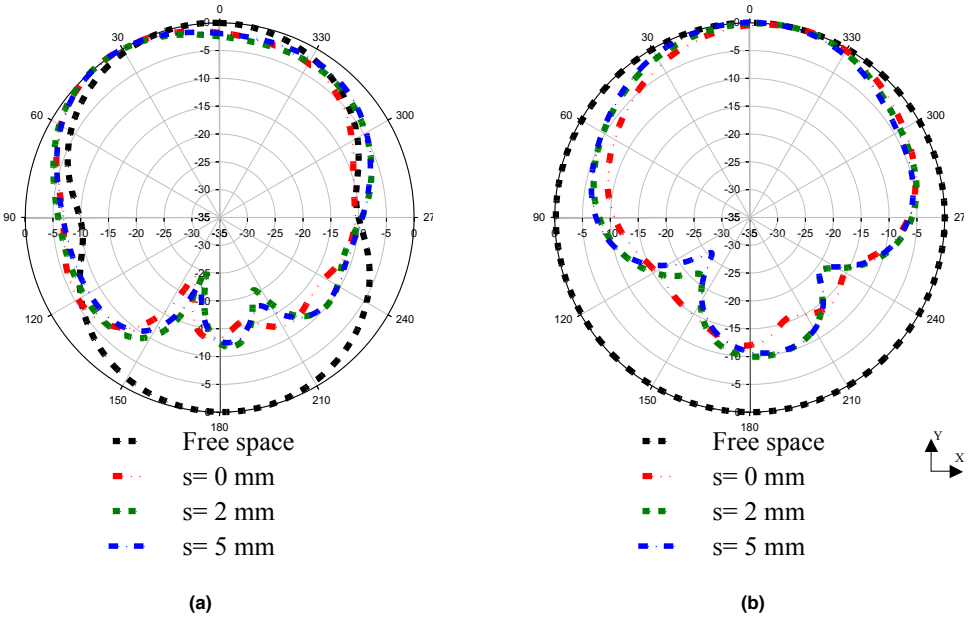

FIGURE 18. Radiation pattern of the CPW antenna alone with varying distance from the multilayer tissue model in the (a) E-plane and (b) H-plane.

B. Human Tissues Loading Evaluation

After investigating the integrated antenna in free space, this section studies the impact on performance of human multilayer tissue. The numerical simulation was conducted using CST. A cuboid of 150 ×150 ×40 mm^3 [47] is utilized to emulate the human chest. The model consists of four layers: bone, muscle, fat and skin. Typical mass density, thickness, conductivity, and permittivity values for each layer are tabulated in Table II [35]. In our full-wave numerical experiment, the space between the integrated antenna and the tissue models is varied, to understand how the EBG-FSS mitigates the human body's loading effect.

TABLE II
PROPERTIES OF THE MODEL TISSUE [35]

	Bone	Muscle	Fat	Skin
Thickness (mm)	13	20	5	2
Density (kg/m^3)	1008	1006	900	1001
σ (S/m)	0.82	1.77	0.11	1.49
ε_r	18.49	52.67	5.27	37.95

Based on Fig. 14(a), the antenna integrated with EBG-FSS possesses a robust input impedance characteristic with S_{11} < -10 dB at the desired frequency, even when it is positioned directly on the multilayer tissue model. S_{11} is very stable with acceptable bandwidth compared to simulation in free space. Conversely, when the antenna is on its own, the impedance performance is sensitive to the separation between the antenna and the tissue. It can be observed that, once the antenna closed to the tissue, S_{11} is most affected, due to the tissue's high dielectric constant of the body. In other words, due to the partial ground of the antenna, the human body is acting as a new complex layer of substrate, therefore mounting the antenna directly on the body causes a dramatic mismatch in the antenna's performance [48].

To validate this, a series of experiments were performed with the antenna with EBG-FSS was directly located on diferent parts of human body such as chest, thigh, and arm as seen in Fig. 15. A male volunteer, weighing 81 kg and height 160 cm, is employed to examine the performance of the prototype design. .

In Fig.16 (a), S_{11} is shown for the case of the integrated antenna when located on different parts of the human body. Similar to what we observed in numerical simulation, for the antenna on human chest, the results showed good agreement between the simulated (Fig. 14 (a)) and measured. In addition, the reasonably stable S_{11} is maintained for the three cases (Fig. 15), with S_{11} maintained < -10 dB. The bandwidth of < -10 dB is maintained, similar to the measured case in free space but slightly broadened. Fig. 16 (b) shows the result of the antenna alone on the same body positions. It is noticed that the center frequency is affected, shifting to lower frequencies, with the bandwidth slightly widened. These trends are also seen during simulation. The slight widening in the bandwidth in both cases results from degraded quality factors of the radiator element caused by the loading by lossy tissue [35].

The radiation pattern performance of the antenna with tissue loading, both integrated and on its own, is seen in Fig. 17 and Fig. 18 in the E-plane and the H-plane respectively The same distances as in Fig. 14 are used to study the radiation pattern. For the case of integrated antenna, the FBR is slightly increased compared to the free space case, since the body acts as an extension of the ground planes and directs the radiation far from the body. On the other hand, with the antenna alone and compared with the case of free space, the

power absorbed by the body is critical, particularly the backward radiation as seen in Fig. 18. Therefore, the whole radiated power is extremely weak. Based on this result it can be concluded that the EBG isolates the body effectively from the radiation. This means that in the presence of EBG-FSS, the antenna can maintain high efficiency and good impedance matching when placed at different distances, even very close to the human body.

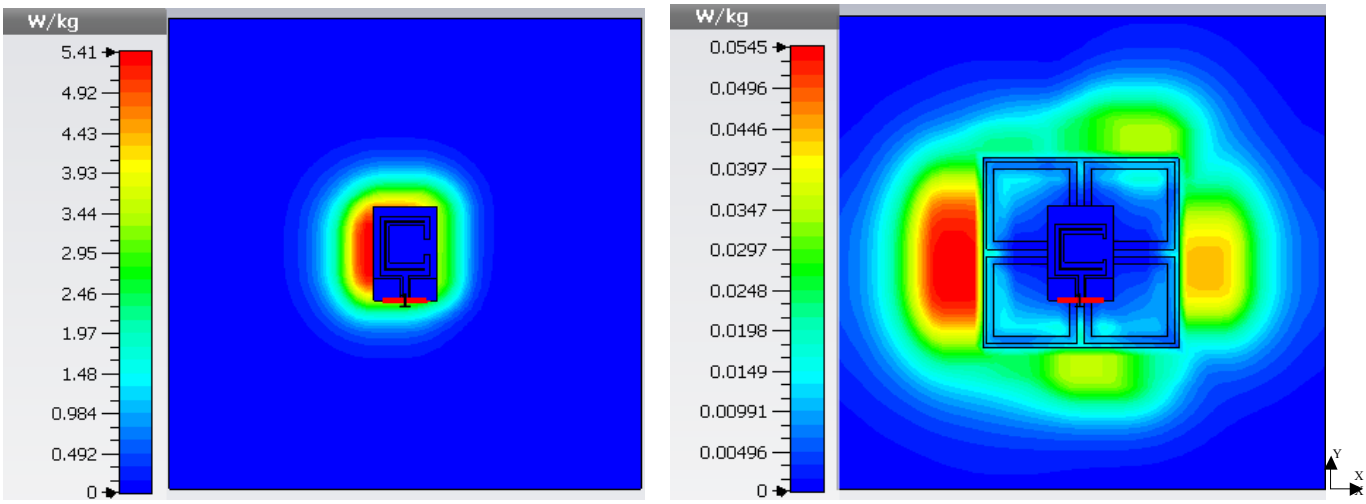

(a) (b)

FIGURE 19. SAR investigation for: (a) antenna alone and (b) integrated antenna at 1 mm from the model.

C. SAR Evaluation

Wearable textile antennas are designed for on-body applications, which means that the antenna must operate near the human body. Thus, SAR is an important factor to calculate when the antenna is excited on the body. SAR values are normally described in units of Watts per kilogram (W/kg).

To investigate the benefits of the EBG-FSS placed between the antenna and the human body, compared with the antenna is alone, a series of SAR simulations were conducted utilizing the human chest model explained in section IV. The model is placed behind the CPW antenna at distances 1, 3 and 5 mm away from the model. Fig. 19 shows the simulated result at 1 mm from the multilayer model. The input power to the antenna is set at 100 mW, and the SAR values determined according to the IEEE C95.1 standards available in the CST MWS software, averaged over 1 g of biological tissue. The SAR levels at 2.4 GHz are summarized in Table III. A noteworthy drop in SAR is realized by using the EBG-FSS structure, as the integrated antenna reduced the SAR levels by more than 95%, thus satisfying the standard.

TABLE III
SAR VALUES AT VARIOUs DISTANCES
FROM THE MODEL TISSUE.

Distance from the phantom (mm)	without EBG-FSS	with EBG-FSS
1	5.41	0.055
3	5.07	0.025
5	4.36	0.015

IV. CONCLUSION

A compact conformal wearable CPW antenna using EBG-FSS for Medical Body Area Network applications at 2.4 GHz is presented. The antenna and EBG-FSS are designed based on fabric materials that can be integrated with our daily clothes. The antenna was studied in free space, on multilayer model tissues and on a real body. The results show that when an antenna on its own, without EBG-FSS, is loaded by human tissue, the frequency detunes: the antenna performs poorly because of the lossy human tissues. Furthermore, the antenna produces a high value of SAR that exceeds the safety limits, due to its omnidirectional radiation pattern resulting in significant backward radiation.Integrating the CPW antenna with an EBG-FSS structure introduces isolation between the body and the antenna. Thus, the detuning due to human body loading, and also the effects of bending, are significantly reduced. Furthermore, the results reveal that the FBR is improved by 13 dB, the gain by 6.55 dBi and the SAR reduced by more than 95% compared to the antenna alone. Therefore, the presented CPW antenna is fit for future wearable MBAN applications.

References

[1] N. A. Malik, M. Ur-Rehman, G. A. Safdar, and Q. H. Abbasi, “Extremely low profile flexible antenna for medical body area networks,” in 2017 IEEE Asia Pacific Microwave Conference (APMC), 2017, vol. Part F1341, no. January, pp. 260–263.

[2] A. Y. I. Ashyap, Z. Z. Abidin, S. H. Dahlan, H. A. Majid, M. R. Kamarudin, and R. A. Abd-Alhameed, “Robust low-profile electromagnetic band-gap-based on textile wearable antennas for medical application,” in 2017 International Workshop on Antenna

Technology: Small Antennas, Innovative Structures, and Applications (iWAT), 2017, pp. 158–161.
[3] H. B. Li, K. i. Takizawa, B. Zhen and R. Kohno, "Body Area Network and Its Standardization at IEEE 802.15.MBAN,"Proc. 16 th IST Mobile and Wireless Comm. Summit, pp. 1-5, 1-5 July 2007.
[4] A. Y. I. Ashyap, Z. Z Abidin, S. Dahlan, H. Majid, S. Shah, M. Kamarudin and A. Alomainy, "Compact and Low-profile Textile EBG-based Antenna for Wearable Medical Applications," IEEE Antennas Wirel. Propag. Lett., vol. 1225, no. c, pp. 1–1, 2017.
[5] G. A. Conway and W. G. Scanlon, "Antennas for Over-Body-Surface Communication at 2.45 GHz," IEEE Trans. on Antennas and Propag., vol. 57, no. 4, pp. 844-855, Apr. 2009.
[6] A. Y. I. Ashyap, W. N. N. W. Marzudi, Z. Z. Abidin, S. H. Dahlan, H. A. Majid, and M. R. Kamaruddin, "Antenna incorporated with Electromagnetic Bandgap (EBG) for wearable application at 2.4 GHz wireless bands," in 2016 IEEE Asia-Pacific Conference on Applied Electromagnetics (APACE), 2016, no. December, pp. 217–221.
[7] H. Cao, V. Leung, C. Chow and H. Chan, "Enabling technologies for wireless body area networks: A survey and outlook," IEEE Communications Magazine, vol. 47, no. 12, pp. 84-93, Dec. 2009.
[8] A. Y. I. Ashap, Z Z Abidin, S H Dahlan, H A Majid, S K Yee, Gameel Saleh, and Norun Abdul Malek, "Flexible Wearable Antenna on Electromagnetic Band Gap using PDMS substrate," TELKOMNIKA ,vol. 15, no. 3, pp. 9–12, 2017.
[9] G. Fang, E. Dutkiewicz, M. A. Huq, R. Vesilo and Y. Yang, "Medical Body Area Networks: Opportunities, challenges and practices," Communications and Information Technologies Intl. Symp., pp. 562-567, Oct. 2011.
[10] B. Lo and G. Z. Yang, "BODY SENSOR NETWORKS – RESEARCH CHALLENGES AND OPPORTUNITIES," Proc. IET Semin. Antennass and Propag. for Body-Centric Wireless Commun., pp. 26-32, 24-24 April 2007.
[11] S. - G. Kim, H.-J. Lee and J.- G. Yook, "A biomolecular sensing platform using RF active system," J. Electromagn. Eng. Sci., vol. 12, no. 4, pp. 227-233, Dec. 2012.
[12] Haiwen Liu, Pin Wen, Shuangshuang Zhu, Baoping Ren, Xuehui Guan, and Hui Yu, "Quad-Band CPW-Fed Monopole Antenna Based on Flexible Pentangle-Loop Radiator," *IEEE Antennas Wirel. Propag. Lett.*, vol. 14, pp. 1373–1376, 2015.
[13] [5] C.-H. Wu, T.-L. Li, M.-H. Hsieh, and J.-S. Sun, "An asymmetric shorted ground using CPW fed antenna for wearable device applications," in *2017 IEEE International Conference on Consumer Electronics - Taiwan (ICCE-TW)*, 2017, pp. 95–96.
[14] Z. Muhammad, S. M. Shah, Z. Z. Abidin, A. Y. I. Asyhap, S. M. Mustam, and Y. Ma, "CPW-fed wearable antenna at 2.4 GHz ISM band," AIP Conference Proceedings 2017, vol. 20003, p. 20003.
[15] A. Alomainy, Y. Hao, A. Owadally, C. G. Parnini, Y. Nechayev, C. C. Constantinou, and P. S. Hall, "Statistical analysis and performanceevaluation for on-body radio propagation with microstrip patch antennas," IEEE Trans. Antennas Propag., vol. 55, no. 1, pp. 245–248, Jan. 2007.
[16] N. Haga, K. Saito,M. Takahashi, and K. Ito, "Characteristics of cavity slotantenna for body-area networks," IEEE Trans. Antennas Propag., vol. 57, no. 4, pp. 837–843, Apr. 2009.
[17] M. N. Suma, P. C. Bybi, and P. Mohanan, "A wideband printed monopole antenna for 2.45 GHz WLAN applications," Microw. Opt. Technol. Lett., vol. 48, no. 5, pp. 871–873, May 2006.
[18] P. S. Hall et al., "Antennas and propagation for on-body communication systems," IEEE Antennas Propag. Mag., vol. 49, no. 3, pp. 41–58, Jun. 2007.
[19] S. Yan, P. J. Soh, and G. A. E. Vandenbosch, "Wearable dual-band magneto-electric dipole antenna for WBAN/WLAN applications," IEEE Trans. Antennas Propag., vol. 63, no. 9, pp. 4165–4169, Sep. 2015.
[20] S. Agneessens and H. Rogier, "Compact half diamond dual-band textile HMSIW on-body antenna," IEEE Trans. Antennas Propag., vol. 62, no. 5, pp. 2374–2381, May 2014.
[21] S. Agneessens, S. Lemey, T. Vervust, and H. Rogier, "Wearable, small, and robust: the circular quarter-mode textile antenna," IEEE Antennas Wireless Propag. Lett., vol. 14, pp. 1482–1485, Jan. 2015.
[22] S. Yan, P. J. Soh, and G. A. E. Vandenbosch, "Dual-band textile MIMO antenna based on substrate-integrated waveguide (SIW) technology," IEEE Trans. Antennas Propag., vol. 63, no. 11, pp. 4640–4647, Nov. 2015.
[23] R. Moro, S. Agneessens, H. Rogier, and M. Bozzi, "Wearable textile antenna in substrate integrated waveguide technology," Electron. Lett., vol. 48, no. 16, pp. 985–986, Aug. 2012.
[24] Z. Wang, L. Z. Lee, D. Psychoudakis, and J. L. Volakis, "Embroidered multiband body-worn antenna for GSM/PCS/WLAN communications," IEEE Trans. Antennas Propag., vol. 62, no. 6, pp. 3321–3329, Jun. 2014.
[25] W. El Hajj, C. Person, and J.Wiart, "A novel investigation of a broadband integrated inverted-F antenna design; application for wearable antenna," IEEE Trans. Antennas Propag., vol. 62, no. 7, pp. 3843–3846, Jul. 2014.
[26] P. J. Soh, G. A. E. Vandenbosch, S. L. Ooi, and N. H. M. Rais, "Design of a broadband all-textile slotted PIFA," IEEE Trans. Antennas Propag., vol. 60, no. 1, pp. 379–384, Jan. 2012.
[27] K. Kamardin, M. K. A. Rahim, P. S. Hall, N. A. Samsuri, T. A. Latef, and M. H. Ullah, "Planar textile antennas with artificial magnetic conductor for body-centric communications," Appl. Phys. A Mater. Sci. Process., vol. 122, no. 4, pp. 1–9, 2016.
[28] S. Zhu and R. Langley, "Dual-band wearable textile antenna on an EBG substrate," IEEE Trans. Antennas Propag., vol. 57, no. 4, pp. 926–935, Apr. 2009.
[29] G.-P. Gao, B. Hu, S.-F. Wang, and C. Yang, "Wearable Circular Ring Slot Antenna With EBG Structure for Wireless Body Area Network," IEEE Antennas Wirel. Propag. Lett., vol. 17, no. 3, pp. 434–437, Mar. 2018.
[30] S. Velan, E. F. Sundarsingh, M. Kanagasabai, A. K. Sarma, C. Raviteja, R. Sivasamy, and J. K. Pakkathillam, "Dual-band EBG integrated monopole antenna deploying fractal geometry for wearable applicaitons", IEEE Ant. Wire. Propag. Lett. Vol. 14, pp. 249-252, 2015.
[31] Z. H. Jiang, Z. Cui, T. Yue, Y. Zhu, and D. H. Werner, "Compact, Highly Efficient, and Fully Flexible Circularly Polarized Antenna Enabled by Silver Nanowires for Wireless Body-Area Networks," IEEE Trans. Biomed. Circuits Syst., vol. 11, no. 4, pp. 920–932, Aug. 2017.
[32] H. R. Raad, A. I. Abbosh, H. M. Al-Rizzo, and D. G. Rucker, "Flexible and compact AMC based antenna for telemedicine applications," IEEE Trans. Antennas Propag., vol. 61, no. 2, pp. 524–531, Feb. 2013.
[33] M. Wang et al., "Investigation of SAR Reduction Using Flexible Antenna with Metamaterial Structure in Wireless Body Area Network," IEEE Trans. Antennas Propag., no. c, pp.
[34] M. A. B. Abbasi, S. S. Nikolaou, M. A. Antoniades, M. Nikolić Stevanović and P. Vryonides, "Compact EBG-backed planar monopole for BAN wearable applications," IEEE Trans. Antennas Propag.,vol. 65, no. 2, pp. 453-463, Feb. 2017.
[35] Z. Jiang, D. E. Brocker, P. E. Sieber, and D. H. Werner, "A compact, low-profile metasurface-enabled antenna for wearable medical body-area network devices," IEEE Trans. Antennas Propag., vol. 62, no. 8, pp. 4021–4030, Aug. 2014.
[36] S. Yan, P. J. Soh, and G. A. E. Vandenbosch, "Low-profile dual-band textile antenna with artificial magnetic conductor plane," IEEE Trans. Antennas. Propag., vol. 61, no. 12, pp. 6487–6490, Dec. 2014.
[37] CST Microwave Studio [Online]. Available: http/www.cst.com.
[38] M. S. Alam, M. T. Islam, and N. Misran, "A Novel Compact Split Ring Slotted Electromagnetic Bandgap Structure for Microstrip Patch Antenna Performance Enhancement," Progress in Electromagnetics Research, Vol. 130, 389-409, 2012.
[39] S. M. Amjadi and M. Soleimani, "A Novel Compact Artificial Magnetic Conductor Based on Multiple Non-grounded Vias," PIERS Online, vol. 2, no. 6, pp. 672–675, 2006.
[40] D. Ferreira, R. F. Caldeirinha, I. Cuinas, and T. R. Fernandes, "Square ˜ loop and slot frequency selective surfaces study for equivalent circuit model optimization," IEEE Trans. Antennas Propag., vol. 63, no. 9, pp. 3947–3955, 2015.

[41] Z. L. Wang, K. Hashimoto, N. Shinohara, and H. Matsumoto, "Frequency-selective surface for microwave power transmission," IEEE Trans. Microw. Theory Tech., vol. 47, no. 10, pp. 2039–2042, Oct. 1999.
[42] F. Yang and Y. Rahmat-Samii, Electromagnetic band gap structures in antenna engineering. *Cambridge University Press*, 2009.
[43] C.L. Holloway, and E.F. Kuester, "Net and partial inductance of a microstrip ground plane," *IEEE Trans. Electromagn. Compat*, vol. 49, pp. 33-46, 1998.
[44] Li Yang, Mingyan Fan, Fanglu Chen, Jingzhao She, and Zhenghe Feng, "A novel compact electromagnetic-bandgap (EBG) structure and its applications for microwave circuits," IEEE Trans. Microw. Theory Tech., vol. 53, no. 1, pp. 183–190, Jan. 2005.
[45] A. Aminian, F. Yang, and Y. Rahmat-Samii, "In-phase reflection and EM wave suppression characteristics of electromagnetic band gap ground planes," *in Proc. IEEE Antennas Propag. Soc. Int. Symp.*, vol. 4, pp. 430–433, Jun 2003.
[46] S. Zhu, "Wearable Antennas for Personal Wireless: PhD thesis," University of Sheffield, 2008.
[47] Z. H. Jiang and D. H. Werner, "Robust low-profile metasurface-enabled wearable antennas for off-body communications," in The 8th European Conference on Antennas and Propagation (EuCAP 2014), 2014, pp. 21–24.
[48] S. Yan, P. J. Soh, and G. A. E. Vandenbosch, "Low-Profile Dual-Band Textile Antenna With Artificial Magnetic Conductor Plane," *IEEE Trans. Antennas Propag.*, vol. 62, no. 12, pp. 6487–6490, Dec. 2014.